

# The estimate of kinetic powers of jets in FR II radio galaxies: existence of invisible components?

Hiroataka Ito<sup>1</sup>, Motoki Kino<sup>2</sup>, Nozomu Kawakatu<sup>3</sup>, Naoki Isobe<sup>4</sup>, and Shoichi Yamada<sup>1,5</sup>

hito@heap.phys.waseda.ac.jp

## ABSTRACT

We investigate the total kinetic powers ( $L_j$ ) and ages ( $t_{\text{age}}$ ) of powerful jets in FR II radio galaxies by comparison of the dynamical model of expanding cocoons with observations. We select four FR II radio sources (Cygnus A, 3C 223, 3C 284, and 3C 219), for which the mass-density profiles of intracluster medium (ICM) are known in the literature. It is found that large fractions  $\gtrsim 0.02 - 0.7$  of the Eddington luminosity ( $L_{\text{Edd}}$ ) are carried away as a kinetic power of jet. The upper limit of estimated  $2L_j/L_{\text{Edd}}$  are larger than unity ( $\lesssim 10$ ) for some sources, suggesting a possibility of super-Eddington mass accretions. As a consequence of the large powers, we also find that the total energy stored in the cocoon ( $E_c$ ) exceeds the energy derived from the minimum energy condition for the energy of radiating non-thermal electrons and magnetic fields ( $E_{\text{min}}$ ):  $4 < E_c/E_{\text{min}} < 310$ . This implies that most of the energy in cocoon is carried by invisible components such as thermal leptons (electron and positron) and/or protons.

*Subject headings:* radiation mechanisms: non-thermal — X-rays: galaxies — radio continuum: galaxies — galaxies: individual (Cygnus A, 3C 223, 3C 284, 3C 219)

---

<sup>1</sup>Science and Engineering, Waseda University, 3-4-1 Okubo, Shinjuku, Tokyo 169-8555, Japan

<sup>2</sup>ISAS/JAXA, 3-1-1 Yoshinodai, 229-8510 Sagamihara, Japan

<sup>3</sup>National Astronomical Observatory of Japan, 181-8588 Mitaka, Japan

<sup>4</sup>Cosmic Radiation Laboratory, Institute of Physical and Chemical Research, Wako, Saitama, Japan 351-0198

<sup>5</sup>Advanced Research Institute for Science & Engineering, Waseda University, 3-4-1 Okubo, Shinjuku, Tokyo 169-8555, Japan

## 1. INTRODUCTION

Relativistic jets in active galactic nuclei (AGN) are a fundamental aspect of plasma accretion onto supermassive black holes (SMBHs). Although the formation mechanism of relativistic jets remains a longstanding problem, it is well established that they carry away some fractions of the available accretion power in the form of collimated beam (e.g., Begelman et al. 1984 for review). The total kinetic powers of AGN jets  $L_j$  is one of the most basic physical quantities characterizing the jet. A lot of authors have investigated  $L_j$  in various ways so far (e.g., Rawlings & Saunders 1991; Celotti & Fabian 1993; Willot et al. 1999). It is, however, difficult to estimate  $L_j$ , since most of the observed emissions from AGN jets are of non-thermal electron origin and it is hard to detect the electromagnetic signals from the thermal and/or proton components. Hence, the free parameter describing the amount of the invisible plasma components always lurks in the estimates of  $L_j$  based on the non-thermal emissions.

The estimate of  $L_j$  for low-power Fanaroff-Riley I (FRI) radio galaxies has been motivated by the observations of “X-ray cavity” which is the region embedded in ICM with the suppressed X-ray surface brightness and coincides with the radio lobe (Böhringer et al. 1993). The cavities (or cocoons) are supposed to be a direct evidence of the displacement of the ambient ICM by the shocked jet matter. Dynamical models of cavities are a good tool, since the invisible plasma components as well as non-thermal electrons play a role for expansions of cavities. For FR I sources, the total kinetic energy of the jet has been estimated as

$$L_j t_{\text{age}} \sim \frac{\hat{\gamma}_c}{\hat{\gamma}_c - 1} P_c V_c,$$

where  $t_{\text{age}}$ ,  $P_c$ ,  $V_c$ ,  $\hat{\gamma}_c$ , are the source age, the pressure, the volume, the adiabatic index of the cavity, respectively (Fabian et al. 2002; Allen et al. 2006). In these studies, however, the thermal pressure of surrounding ICM ( $P_{\text{ICM}}$ ) is substituted for the one in the cavity (i.e.,  $P_c \sim P_{\text{ICM}}$ ). This assumption may be applied only to subsonic expansions.

On the other hand, the cocoon pressure of powerful Fanaroff-Riley class II (FR II) radio galaxies is expected to be larger than that of the surrounding ICM, which is expressed as  $P_c > P_{\text{ICM}}$  (Begelman & Cioffi 1989 hereafter BC89), and the cocoon of FR II radio galaxies is likely to be expanding super-sonically. Then the substitution of ICM pressure for the cocoon pressure is not justified. A new estimate of  $L_j$  for FR II radio galaxies by use of the dynamical model of cocoon expansions is proposed by Kino & Kawakatu (2005) (hereafter KK05), in which  $L_j$  and  $t_{\text{age}}$  are derived from the comparison of the cocoon model with the morphology of the cocoon obtained by radio observations. It should be stressed that  $P_c$  is not assumed but solved in this model. Hence it can be applied even to the cocoons with

$P_c > P_{\text{ICM}}$ . So far, however, this estimate of  $L_j$  has been applied only to Cygnus A. The expansion of the number of samples is evidently crucially important for exploring general characteristics of the powerful AGN jets. For this purpose, we apply the method of KK05 to other bright FR II radio galaxies, for which the physical conditions of the associated ICM have been estimated in the literature.

In the present work, we especially focus on the ratio of  $L_j/L_{\text{Edd}}$ , where  $L_{\text{Edd}}$  is the Eddington luminosity of AGN, since  $L_j/L_{\text{Edd}}$  is a more fundamental quantity than  $L_j$  from the point of view of the jet formation physics. Another interesting quantity we examine in this work is the ratio of the internal energy deposited in the cocoon ( $E_c$ ) to the minimum energy ( $E_{\text{min}}$ ) obtained by the minimum energy condition for radiating non-thermal electrons and magnetic fields (e.g., Miley 1980). Some of the previous works studying this quantity (e.g., Hardcastle & Worrall 2000; Leahy & Gizani 2001) reported that the cocoon pressure expected from the inferred  $E_{\text{min}}$  is smaller than the pressure of ambient matter, suggesting the difference between  $E_c$  and  $E_{\text{min}}$ . due to the lack of minimum pressure against the pressure of ambient medium. Although these studies obtained the lower limit of the ratio, it is the value of  $E_c$  that is of greater importance.

According to a large sample of galaxies collected recently, the fraction of AGNs in all the galaxies is suggested to be  $\sim 20\text{--}40\%$ , larger than previously thought (Kauffman et al. 2003; Miller et al. 2003). The interest in AGNs is gaining momentum in the context of the co-evolution of galaxies and their central black holes (e.g., Kawakatu et al. 2003, Granato et al. 2004; Di Matteo et al. 2005). AGN outflows in particular are likely to be a key ingredient in this context (Silk & Rees 1998; Fabian 1999; King 2003). The AGN feedback by the outflows may be also promising to explain the tight correlations between the ratio of the mass of SMBH ( $M_{\text{BH}}$ ) to that of galactic bulge (Kormendy & Richstone 1995; Magorrian et al. 1998) and the ratio of  $M_{\text{BH}}$  and the stellar velocity-dispersion in the bulge (Ferrarese & Merritt 2000; Tremaine et al. 2002). In this sense, a robust estimate of the basic quantities such as  $L_j/L_{\text{Edd}}$  and  $t_{\text{age}}$  of radio loud AGNs at low  $z$  is an important first step for understanding the AGN feedback processes in the universe.

The outline of the paper is as follows. In §2, the model of the expanding cocoon by KK05 is briefly reviewed. In §3, we explain how to extract the key quantities from the observations of four nearby FR II radio galaxies, Cygnus A, 3C 223, 3C 284, and 3C 219, which are required for the comparison with the model. We then estimate the total kinetic power,  $L_j$ , and the dynamical ages,  $t_{\text{age}}$ , in §4. Finally in §5, we summarize our results and discuss some implications on the physics of AGN jet. Throughout the paper, we adopt a cosmology with  $H_0 = 71 \text{ km s}^{-1}$ ,  $\Omega_M = 0.3$ , and  $\Omega_\Lambda = 0.7$  (Spergel et al. 2003).

## 2. COCOON MODEL

### 2.1. Basic equations

Based on BC89 and KK05, we briefly summarize the cocoon model we employ in the following. We focus on the cocoon expansion in the over-pressured regime, namely  $P_c > P_a$ , where  $P_c$  and  $P_a$  are the pressures of cocoon and ambient ICM, respectively. We approximately describe the expansion of cocoon by the following three equations: (1) the equation of the motion along the jet axis, (2) the equation for the sideways expansion, and (3) the energy equation. They are expressed, respectively, as

$$\frac{L_j}{v_j} = \rho_a(r_h) v_h^2(t) A_h(t), \quad (1)$$

$$P_c(t) = \rho_a(r_c) v_c(t)^2, \quad (2)$$

$$\frac{dE_c(t)}{dt} + P_c(t) \frac{dV_c(t)}{dt} = 2L_j, \quad (3)$$

where  $v_j$ ,  $\rho_a$ ,  $v_h$ ,  $v_c$ , and  $A_h$  are the velocity of jet, the density of ambient medium, the advance velocity of cocoon head, the velocity of sideways expansion, and the cross sectional area of cocoon head, respectively. Here  $E_c = P_c V_c / (\hat{\gamma}_c - 1)$  is the total internal energy deposited in the cocoon, where  $\hat{\gamma}_c$  is the specific heat ratio of the plasma inside cocoon. The cocoon shape is approximated as a spheroid, and its volume is given as  $V_c(t) = (4\pi/3)r_c(t)^2 r_h(t)$ . The distance from the jet apex to the hot spot and the radius of cocoon body are obtained from  $r_h(t) = \int_{t_{\min}}^t v_h(t') dt'$  and  $r_c(t) = \int_{t_{\min}}^t v_c(t') dt'$ , respectively, and  $t_{\min}$  is the initial time of source evolution. Throughout this paper, we assume  $\hat{\gamma}_c = 4/3$ , since the cocoon is expected to be dominated by relativistic particles (Kino et al. 2007). In these equations we also assume that the jet has a relativistic velocity ( $v_j \sim c$ ) and that  $L_j$  is constant in time. The mass density of ICM,  $\rho_a$ , is assumed to be given by  $\rho_a(r) = \bar{\rho}_a (r/r_0)^{-\alpha}$ , where  $r_0$  and  $\bar{\rho}_a$  are the reference position and the ICM mass density at  $r_0$ , respectively. We set  $r_0$  to be  $r_h(t_{\text{age}})$ , where  $t_{\text{age}}$  is the present age of cocoon, throughout this paper. A cartoon of the cocoon model is illustrated in Fig. 1. In this paper, we have slightly improved the model of BC89 and KK05 as follows: (i) a more accurate definition of  $V_c$  is employed, and (ii) the  $PdV$  work, which is done by the cocoon against the contact discontinuity between the cocoon and the shocked ambient medium, is taken into account. These corrections are necessary in the following quantitative estimate of  $L_j$ . In fact, the estimated power is reduced by a factor of  $\sim 50$  from the value in KK05 for Cygnus A after taking account of the corrections (see §2.4 for details).

The model parameters are  $L_j$  and  $t$ , and the unknown physical quantities are  $v_h$ ,  $v_c$ ,  $P_c$ , and  $A_h$ . Since the number of unknown quantities is four, while that of basic equations is three, an additional condition is required for the system of equations to be closed. Here we assume that the cross sectional area of cocoon body  $A_c = \pi r_c^2$  is given by  $A_c(t) \propto t^X$  and treat  $X$  as a free parameter which is determined by the imposed condition. Once the value of  $X$  is determined, we obtain  $v_h$ ,  $v_c$ ,  $P_c$ , and  $A_h$  as a function of  $L_j$  and  $t$ . It is worth noting that the model is capable of producing various dynamics by tuning the value of  $X$ . For example, the results of 2D relativistic hydrodynamical simulations by Scheck et al. (2002) were reproduced fairly well in Kawakatu & Kino (2006).

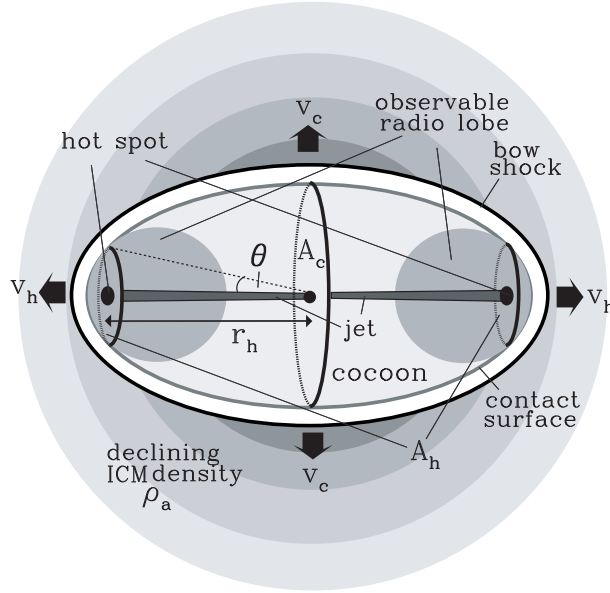


Fig. 1.— A cartoon of the employed model. The relativistic jet from FR II radio galaxy interacts with ICM with a declining density. Most of the kinetic energy of jet is deposited in the cocoon, which is then inflated by the internal energy.

## 2.2. Analytical solution

We assume that the physical quantities have a power-law time-dependence of the form  $A = \bar{A} (t/t_{\text{age}})^Y$ , where  $Y$  is the power-law index. Then the index and coefficient of  $v_c$ , for example, are determined as

$$v_c(t) = \bar{v}_c \left( \frac{t}{t_{\text{age}}} \right)^{0.5X-1} = \frac{\bar{A}_c^{1/2}}{t_{\text{age}}} \mathcal{C}_{\text{vc}} \left( \frac{t}{t_{\text{age}}} \right)^{0.5X-1}. \quad (4)$$

From this relation and Eqs. (1)-(3), we obtain the following expressions:

$$P_c(t) = \bar{\rho}_a \bar{v}_c^2 \mathcal{C}_{pc} \left( \frac{\bar{v}_c}{v_0} \right)^{-\alpha} \left( \frac{t}{t_{\text{age}}} \right)^{X(1-0.5\alpha)-2}, \quad (5)$$

$$v_h(L_j, t) = \frac{L_j}{\bar{\rho}_a \bar{v}_c^2 \bar{A}_c} \mathcal{C}_{vh} \left( \frac{\bar{v}_c}{v_0} \right)^{\alpha} \left( \frac{t}{t_{\text{age}}} \right)^{X(-2+0.5\alpha)+2}, \quad (6)$$

$$A_h(L_j, t) = \frac{L_j}{v_j \bar{\rho}_a \bar{v}_h^2} \mathcal{C}_{ah} \left( \frac{\bar{v}_h}{v_0} \right)^{\alpha} \left( \frac{t}{t_{\text{age}}} \right)^{X(\alpha-2)(-2+0.5\alpha)+3\alpha-4}, \quad (7)$$

where  $\mathcal{C}_{vh} = 0.75(\hat{\gamma}_c - 1)(0.5X)^{-\alpha}[3 - (2 - 0.5\alpha)X]/[X(-1 + 0.5\alpha)(\hat{\gamma}_c - 1) + 3\hat{\gamma}_c - 2]$ ,  $\mathcal{C}_{vc} = 0.5X/\pi^{1/2}$ ,  $\mathcal{C}_{pc} = (0.5X)^{\alpha}$ , and  $\mathcal{C}_{ah} = [X(-2 + 0.5\alpha) + 3]^{-\alpha}$ , and  $v_0 \equiv r_h(t_{\text{age}})/t_{\text{age}}$  corresponds to the head speed assumed to be constant in time. The difference in  $\mathcal{C}_{vh}$  obtained here from that in KK05 is due to the correction made in Eq. (3). We assume the conditions of  $0.5X > 0$  and  $X(-2 + 0.5\alpha) + 3 > 0$ , which ensure that the contribution at  $t_{\text{min}}$  to the integrations of  $r_h$  and  $r_c$  is small enough. The cases that we focus on in §3 clearly satisfy these conditions.

### 2.3. Determination of $X$

As mentioned in §2.1, an additional condition that determines the free parameter  $X$  is required for the system of equations to be closed. In the pioneering study of BC89,  $A_h(t) = \text{const}$  was assumed. However, as can be confirmed from numerical simulations (e.g., Cioffi & Blondin 1992; Scheck et al. 2002), it is obvious that this condition is unlikely to hold for long-term evolutions from pc to Mpc scales. In this paper, we consider the following two conditions, which seem more reasonable and equally possible, in determining  $X$ :

- **Constant aspect ratio** (Case I)

The aspect ratio of cocoon,  $\mathcal{R} = r_c/r_h$ , is assumed to be constant in time. This corresponds to the widely-discussed self-similar evolution (Begelman 1996; Komissarov & Falle 1997; Kaiser & Alexander 1997; Bicknell et al. 1997). Since the time dependence of  $\mathcal{R}$  is given by  $\mathcal{R}(t) \propto t^{[X(2.5-0.5\alpha)-3]}$ , we obtain  $X = 6/(5 - \alpha)$  in this case.

- **Constant opening angle** (Case II)

The opening angle,  $\theta = \tan^{-1}(A_h^{1/2}/\pi^{1/2}r_h)$  (see Fig. 1), is assumed to be constant in time. Although there has been no previous work that has employed this condition, it

seems to be reasonable when the jet is precessing with a constant pitch angle. Since the time dependence of  $\tan\theta$  is given by  $\tan\theta(t) \propto t^{[0.25X(\alpha-4)^2+1.5\alpha-5]}$ ,  $X = (20 - 6\alpha)/(4 - \alpha)^2$  is obtained for this case.

It should be emphasized here that these two independent conditions lead to the solutions that describe quite similar dynamical evolutions as long as the range of  $\alpha$  listed in Table 1 is adopted ( $1 \leq \alpha \leq 2$ ). This can be seen as follows. If the constant opening angle is imposed (Case II), the evolution of the aspect ratio is obtained as  $\mathcal{R}(t) \propto t^{(2-\alpha)/(4-\alpha)^2}$ . It is easy to confirm its very weak time dependence, since the power-law index is limited to the range  $0 \leq (2 - \alpha)/(4 - \alpha)^2 \leq 1/9$ . Just in the same way, if the constant aspect ratio is adopted (Case I), we find again a very weak time dependence of the opening angle,  $\tan\theta(t) \propto t^{(\alpha-2)/[2(5-\alpha)]}$ , with the power-law index being  $-1/8 \leq (\alpha - 2)/[2(5 - \alpha)] \leq 0$ .

As a consequence of this small difference between the two solutions, the corresponding values of  $X$  also show only a slight difference. For example, when a typical value  $\alpha = 1.5$  is taken, we obtain  $X = 12/7 \sim 1.71$  and  $X = 1.76$  for Case I and Case II, respectively. Hence, the estimated  $L_j$  and  $t_{\text{age}}$  based on these two sets of solutions also do not vary much, either. Indeed, for the given values of  $r_h$ ,  $A_h$ , and  $\mathcal{R}$ , the derived  $L_j$  and  $t_{\text{age}}$  only differ by a factor of  $\sim 1.7$  and  $\sim 0.83$ , respectively, between the two cases for  $\alpha = 1.5$ . It is worth noting that for  $\alpha = 2$ , which corresponds to the 3C 219 (Table 1), the two conditions give the same value of  $X = 2$  and, as a result, the solutions are identical. Since only a slight change is found between the two cases, we focus on the widely-discussed self-similar solution (Case I) in the following.

## 2.4. Improvements from KK05

In the present study, we have improved the energy equation given in KK05 for more accurate quantitative estimations of  $L_j$  and  $t_{\text{age}}$ . As mentioned in §2.1, the resultant change in the derived  $L_j$  turns out to be rather large. Here we explain the reasons for this discrepancy more in detail.

As mentioned in §2.1, we have (i) modified  $dV_c/dt$  and (ii) included the  $PdV$  term in Eq. (3). As for (i), the main flaw in KK05 is the fact that they did not take into account the sideways expansion in the growth of  $V_c$ . In fact, they employed the equation,  $dV_c/dt = 2\pi r_c^2 v_h$ , whereas a more accurate expression is  $dV_c/dt = (4/3)[\pi r_c^2 v_h + 2\pi r_c r_h v_c]$ , which is adopted in the present study. As for (ii), it was assumed that all injected energy is converted to internal energy (namely,  $E_c = 2L_j t_{\text{age}}$ ) in KK05. It is obvious, however, that a part of the injected energy is consumed for expansions and the  $PdV$  work should be

included, particularly for quantitative estimations. As found in §2.2, these corrections are reflected only in the numerical factor  $\mathcal{C}_{\text{vh}}$  in Eq. (6). The value of  $\mathcal{C}_{\text{vh}}$  is reduced by a factor of  $\sim 3.5$  owing to (i) and another factor of  $\sim 2$  due to (ii) and, hence, by a factor of  $\sim 7$  as a whole. For a given geometry of cocoon ( $r_{\text{h}}$ ,  $A_{\text{h}}$ , and  $\mathcal{R}$ ) and ambient density profile ( $\rho_{\text{a}}$  and  $\alpha$ ), the derived power and age scale with the numerical factor as  $L_{\text{j}} \propto \mathcal{C}_{\text{vh}}^2$  and  $t_{\text{age}} \propto \mathcal{C}_{\text{vh}}^{-1}$ , respectively. As a result, KK05 overestimated  $L_{\text{j}}$  by a factor of  $\sim 50$ . On the other hand,  $t_{\text{age}}$  was underestimated by a factor of  $\sim 0.14$ , which led to the overestimation of  $E_{\text{c}}$  by a factor of  $\sim 14$ , since the latter is obtained as  $E_{\text{c}} = 2L_{\text{j}}t_{\text{age}}$  in KK05. It is also worthy to note that in the present study the following relation holds:  $E_{\text{c}} \simeq L_{\text{j}}t_{\text{age}}$ . The difference of the factor  $\sim 2$  arises from the fact that about a half of the injected energy is used for the  $PdV$  work.

### 3. EXTRACTION OF THE KEY QUANTITIES FROM THE OBSERVATIONS

In determining  $L_{\text{j}}$  and  $t_{\text{age}}$ , we essentially follow the same procedure taken in KK05. In this section, we explain in detail how to extract the key quantities utilized in the model from the observations.

#### 3.1. ICM quantities

As for the mass-density profiles ( $\rho_{\text{a}}$ ) and pressures ( $P_{\text{a}}$ ) of ICM, we adopt the values given in the literature (Reynolds & Fabian (1996); Smith et al. (2002) for Cygnus A, Croston et al. (2004) for 3C 223 and 3C 284, and Hardcastle & Worrall (1999) for 3C 219). In these papers, the X-ray surface brightness distribution of ICM was fitted by the isothermal  $\beta$ -model, which takes the form of  $\rho(r) = \rho_{\text{core}}[1 + (r/r_{\text{core}})^2]^{-3\beta/2}$  (Cavaliere & Fusco-Femiano 1978), where  $\rho_{\text{core}}$  and  $r_{\text{core}}$  are the core radius and density of the ICM, respectively. Since we employ the density profile of  $\rho_{\text{a}}(r) = \bar{\rho}_{\text{a}}(r/r_{\text{h}})^{-\alpha}$  in our model, a power-law approximation of the  $\beta$ -model is necessary. In the present study, we determine  $\bar{\rho}_{\text{a}} = \rho_{\text{a}}(r_{\text{h}})$  and  $\alpha$  from the  $\beta$ -model as follows. The determination of  $\bar{\rho}_{\text{a}}$  is done simply by equating it with the density in the  $\beta$ -model at the corresponding radius  $r_{\text{h}}$ , namely  $\bar{\rho}_{\text{a}} = \rho_{\text{core}}[1 + (r_{\text{h}}/r_{\text{core}})^2]^{-3\beta/2}$ . In the case of  $r_{\text{h}} \gg r_{\text{core}}$ , it is clear that  $\alpha$  can be approximated by  $3\beta$ . Only Cygnus A satisfies this condition, though. For the rest of the sources,  $r_{\text{h}}$  is comparable to  $r_{\text{core}}$ :  $r_{\text{core}} \sim 340$  kpc, 210 kpc, and 90 kpc for 3C 223, 3C 284, and 3C 219, respectively. It is obvious that the above approximation of  $\alpha \approx 3\beta$  would cause an overestimation of density gradient for these cases. Instead  $\alpha$  should be taken to be a typical value in the ICM region swept by the



expanding cocoon. Here we determine  $\alpha$  by requiring that  $\rho_a(r)$  should coincide with the density in the  $\beta$ -model at  $r = 0.5r_h$  in addition to  $r = r_h$ . Although there is no compelling reason for the choice of  $r = 0.5r_h$ , the estimations of  $L_j$  and  $t_{\text{age}}$  are affected little by this uncertainty (§4.1). Once  $\rho_a$  is given,  $P_a$  is obtained by the equation of state, which is written as  $P_a(r) = \frac{k_B T_a}{\mu m_H} \rho_a(r)$ , where  $T_a$  and  $\mu = 0.6$  are the temperature and mean molecular weight of ICM, respectively, and  $m_H$  is the mass of hydrogen. We adopt the temperature used in the  $\beta$ -model, ignoring the radial dependence of  $T_a$  as usual. In Table 1, we list the values of  $\rho_a$  and  $P_a$  at  $r = r_h$  and  $\alpha$  for each source.

### 3.2. $r_h$ and $A_h$

In Fig. 3, we show the VLA images of Cygnus A (Perley et al. 1984), 3C 223 (Leahy & Perley 1991), 3C 284 (Leahy et al. 1986), and 3C 219 (Clarke et al. 1992) in logarithmic scale. Contours in linear scale are also displayed to determine the position of hot spot accurately. The overlaid straight lines that cross each other at right angle on the hot spot are the lines we use to measure  $r_h$  and  $A_h$ . For simplicity, we neglect the projection effect of  $r_h$ , which would be at most a factor of a few if we believe the unified model of AGN (Urry & Padovani 1995).  $A_h$  is measured as a cross-sectional area of the radio lobe at the position of the hot spot.  $r_h$  and  $A_h$  for each source are summarized in Table 1.

It should be noted that the plasma just around the hot spot is very fresh in the sense that a significant synchrotron cooling is absent. Hence, the effect of radiative cooling does not introduce large ambiguity in the estimation of  $A_h$ . The adiabatic cooling, on the other hand, is not expected to cause any problem in the estimation for the following reason. Since the sound crossing time in the head region of the cocoon,  $\sim A_h^{1/2}/c_s$ , where  $c_s = c/\sqrt{3}$  is the sound speed, is much shorter than the age of the cocoon, we can regard the head region to be uniform to the lowest order. Hence, the adiabatic cooling, if any, would decrease the surface brightness gradually as the distance from the hot spot increases. Contrary to this, the observed radio images show a sharp decline of the surface brightness at the outer edge, which is most naturally interpreted as the existence of the periphery of cocoon head there.

Next we address the issue in determining  $A_h$  that arises from multiple hot spots. Double hot spots are actually observed in the radio lobes of Cygnus A (see, e.g., Carilli & Barthel 1996). In determining  $A_h$ , we adopt the “disconnected-jet” model by Cox et al. (1991) to Cygnus A. The double hot spots are referred to as primary and secondary as follows. The primary hot spot is more compact and located in the inner part of the lobe, whereas the secondary spot is more diffuse and brighter and located in the outer part of the lobe. According to the disconnected-jet model, double hot spots are produced by the sudden

change of the jet-orientation, or the disconnection, which leads to the termination of energy supply to the original shock and the generation of a new jet. While the primary hot spot is produced by the terminal shock in the new jet, the secondary hot spot remains as a relic in the original jet. The schematic picture of the model is illustrated in Fig. 2. Since the primary hot spot is predicted to be much younger than the source age, we employ the position of the secondary hot spot to determine  $A_h$ . We will discuss this point more in detail in the following.

The age of Cygnus A is roughly estimated to be  $t_{\text{age}} \approx r_h/\beta_{\text{hs}}c \approx 2.0 \times 10^7 (\beta_{\text{hs}}/10^{-2})^{-1}$  yr, where  $\beta_{\text{hs}}c$  is the advance velocity of the hot spot. On the other hand, since the primary hot spot is observed simultaneously with the secondary hot spot, its age should be younger than the duration,  $t_{\text{dur}}$ , in which the secondary spot is bright.  $t_{\text{dur}}$  is expressed as a sum of the time up to the shut-off of the energy supply from the disconnected-jet to the spot,  $t_{\text{dis}}$ , and the cooling time,  $t_{\text{cool}}$ :

$$t_{\text{dur}} = t_{\text{dis}} + t_{\text{cool}} \approx \max(t_{\text{dis}}, t_{\text{cool}}). \quad (8)$$

The cooling time is evaluated as  $t_{\text{cool}} = \min(t_{\text{syn}}, t_{\text{ad}})$ , where  $t_{\text{syn}}$  and  $t_{\text{ad}}$  are the synchrotron cooling timescale and the adiabatic expansion timescale, respectively. A typical value of  $t_{\text{syn}}$  at the hot spot is estimated as  $t_{\text{syn}} \approx 1.0 \times 10^6 (B/10^{-4}\text{G})^{-3/2} (\nu/1\text{ GHz})^{-1/3}$  yr, whilst  $t_{\text{ad}}$  is given by  $t_{\text{ad}} \approx r_{\text{hs}}/c_s = 5.6 \times 10^3 (r_{\text{hs}}/1\text{kpc})$  yr, where  $r_{\text{hs}}$  is the size of the hot spot. These estimates lead to  $t_{\text{cool}} = t_{\text{ad}}$  for the secondary hot spot. On the other hand,  $t_{\text{dis}}$  is given by  $t_{\text{dis}} = r_{\text{dis}}/v_j$ , where  $r_{\text{dis}}$  is the distance from the tail to the hot spot in the disconnected jet. Although we do not know  $r_{\text{dis}}$  from observations, we can at least put the upper limit as  $r_h > r_{\text{dis}}$ . We then obtain  $t_{\text{dis}} < 2.0 \times 10^5 (r_h/60\text{ kpc})(v_j/c)^{-1}$  yr. Hence, from Eq. (8), we see that  $t_{\text{dur}}$  is in the range  $\sim 5 \times 10^3 - 2 \times 10^5$  yr. From these estimates, it is obtained that the age of the primary hot spot only makes up a small fraction of its whole lifetime. Therefore, we adopt the secondary spot for the determination of  $A_h$ , which reflects the whole evolution of the cocoon (Fig. 3).

### 3.3. $\mathcal{R}$

In contrast to  $r_h$  and  $A_h$ , it is difficult to measure the aspect ratio of cocoon,  $\mathcal{R}$ , from the VLA radio images, since the cocoon emission from the region far away from the hot spot is very dim at GHz frequency because of the synchrotron cooling (see Fig. 3). It is well known that this cooling effect can be used to infer the age of radio galaxy (the spectral ageing method, e.g., Carilli et al. 1991). As one utilizes lower frequencies, however, the cocoon image is expected to be thicker, since lower-energy electrons have longer synchrotron cooling

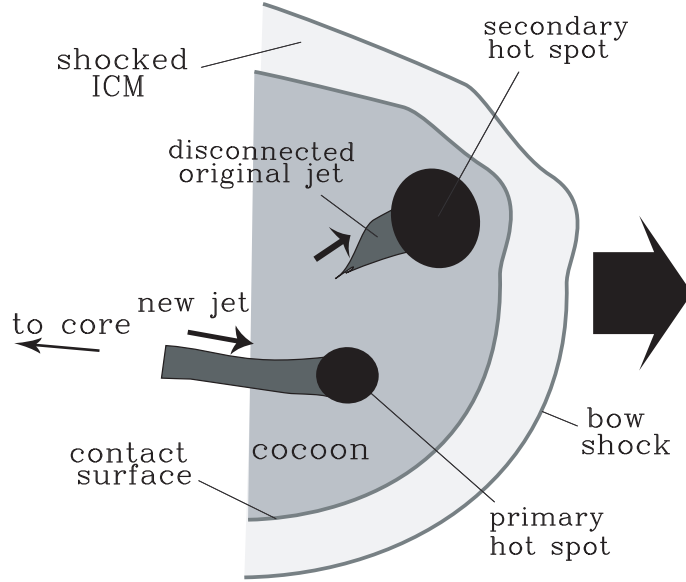


Fig. 2.— A cartoon around the double hot spots in the “disconnected-jet” model. As a result of altering orientation, jet becomes disconnected and forms the primary and the secondary hot spot which are the location of the present and the previous terminal shock, respectively.

times (e.g., Carilli and Barthel 1996). In fact, a few authors have reported the existence of prolate cocoons, based on the observations at a relatively low radio frequency (610 MHz) band (e.g., Readhead et al. 1996). It is mentioned, however, that little attention has been paid to observational features concerning the structure of cocoons so far.

On the other hand, theoretical studies of jet propagation and cocoon formation with multi-dimensional hydrodynamic simulations clearly support the existence of cocoon for reasonably light beams going through surrounding ICM (Scheck et al. 2002; Aloy et al. 2000; Gomez et al. 1997; Komissarov & Falle 1997; Mioduszewski et al. 1997). The intensity maps of the synchrotron emissivities obtained in these hydrodynamical simulations well reproduce the double lobe structures as observed (e.g., Fig. 10 in Scheck et al. 2002). It seems natural, therefore, to suppose that cocoons are commonly produced, although there is a room for further observational investigations. In the present study, we explore a wide range of  $0.5 < \mathcal{R} < 1$  in order to take account of the large ambiguity on the shape of cocoon. It is worthwhile to note in this respect that the existence of cocoon can be confirmed for Cygnus A in the Chandra image (Wilson et al. 2000, 2006) and that the obtained aspect ratio  $\sim 0.5 - 0.7$  lies in the range explored in this paper.

## 4. RESULTS

### 4.1. Total kinetic power and dynamical age

The resultant  $L_j$  and  $t_{\text{age}}$  are displayed in Figs. 4, 5, 6, and 7. Since most of the radio sources show asymmetries in the pair of lobes, we analyze each lobe independently. Three oblique lines in these figures are the obtained  $L_j$  and  $t_{\text{age}}$  for different  $\alpha$ 's, and their ranges reflect the uncertainty in  $\mathcal{R}$ . The thick solid line shows the result for the parameter set listed in Table 1. The other two lines correspond to the results obtained by varying  $\alpha$  by  $\pm 0.5$ . From the figures, it is confirmed that the results are rather insensitive to the value  $\alpha$ . In each line, the power and age depend on the aspect ratio  $\mathcal{R}$  as  $L_j \propto \mathcal{R}^{2\alpha-8}$  and  $t_{\text{age}} \propto \mathcal{R}^{4-\alpha}$ , and, therefore, satisfy  $L_j \propto t_{\text{age}}^{-2}$ . Since  $\alpha$  does not exceed 4 in any of the four sources, a lower aspect ratio corresponds to a higher power with a lower age. It should be noted that the uncertainty in the absolute values of  $\rho_a$  and  $P_a$  is not crucial, since  $P_a$  is used only to judge whether the over-pressure condition is satisfied or not, and the dependence of  $L_j$  and  $t_{\text{age}}$  on  $\rho_a$  is rather weak,  $L_j \propto \rho_a$  and  $t_{\text{age}} \propto \rho_a^0$ . The line outside the shaded region must be discarded, since the over-pressure condition is violated. The Eddington luminosity,  $L_{\text{Edd}}$ , of each source is also shown in these figures for comparison. In Table 3, we summarize the allowed values of  $L_j$  and  $t_{\text{age}}$  and other relevant physical parameters of cocoon obtained for the parameter set listed in Table 1.

Cygnus A is one of the vastly studied nearby FR II radio galaxies. Tadhunter et al. (2003) estimated the SMBH mass of Cygnus A as  $2.5 \times 10^9 M_\odot$ , based on the gas kinematics in the narrow-line region. Its linear size is measured as  $r_h = 70$  kpc for the western jet and  $r_h = 60$  kpc for the eastern jet. From the employed values of  $r_h$  and  $A_h$ , the power and age are obtained as  $L_j = (0.35 - 1.1) \times 10^{46}$  ergs  $\text{s}^{-1}$  and  $t_{\text{age}} = 30 - 53$  Myr for the western jet and  $L_j = (0.4 - 2.6) \times 10^{46}$  ergs  $\text{s}^{-1}$  and  $t_{\text{age}} = 19 - 47$  Myr for the eastern jet. No significant difference is seen between the two jets, and we interpret that the actual age lies in these ranges. Note that  $L_j$  is decreased and  $t_{\text{age}}$  is increased from those in KK05 by the improvement of  $V_c$  and the inclusion of  $PdV$  work. In fact, while  $L_j = 1.3 \times 10^{48}$  ergs  $\text{s}^{-1}$  and  $t_{\text{age}} = 2.6$  Myr were obtained in KK05, we find  $L_j = 2.6 \times 10^{46}$  ergs  $\text{s}^{-1}$  and  $t_{\text{age}} = 19$  Myr in this paper when the identical values of  $r_h = 60$  kpc,  $A_h = 150 \text{ kpc}^2$ , and  $\mathcal{R} = 0.5$  are employed.

3C 223 has radio lobes that extend up to  $r_h = 340$  kpc in both sides. Its SMBH mass is estimated as  $1.4 \times 10^8 M_\odot$  by Woo & Urry (2002), based on the observed stellar velocity dispersions. As can be seen in Fig. 3, 3C 223 has asymmetry in  $A_h$ . While a well developed cocoon head is seen at the northern hot spot ( $A_h = 4300 \text{ kpc}^2$ ), the cocoon head at the southern hot spot is quite compact ( $A_h = 1800 \text{ kpc}^2$ ). Reflecting this asymmetry,

the obtained power and age show quite large difference:  $L_j = (0.15 - 2.9) \times 10^{46}$  ergs s<sup>-1</sup> and  $t_{\text{age}} = 140 - 610$  Myr for the northern jet, and  $L_j = (0.71 - 2.0) \times 10^{45}$  ergs s<sup>-1</sup> and  $t_{\text{age}} = 330 - 560$  Myr for the southern jet.

3C 284 shows asymmetry both in  $r_h$  and  $A_h$ . While  $r_h$  and  $A_h$  in the western lobe are estimated as 380 kpc and 6200 kpc<sup>2</sup>, respectively, the corresponding values for the eastern lobe are 260 kpc and 4600 kpc<sup>2</sup>. The obtained power and age are  $L_j = (0.1 - 3.6) \times 10^{46}$  ergs s<sup>-1</sup> and  $t_{\text{age}} = 100 - 630$  Myr for the western jet and  $L_j = (0.03 - 1.8) \times 10^{47}$  ergs s<sup>-1</sup> and  $t_{\text{age}} = 32 - 260$  Myr for the eastern jet. Since there is no estimate of the SMBH mass of 3C 284 in the literature, we derive the mass from the B-band magnitude of the buldge estimated in Shi et al. (2005). By using the equation in Marchesini et al. (2004) which gives the correlation of the B-band magnitude with the BH mass, we obtain  $M_{\text{BH}} = 8.2 \times 10^8 M_\odot$ .

In the case of 3C 219, we only analyze the jet on the western side, since the eastern lobe shows severe deformation (see Fig. 3). We could not determine  $A_h$  on the eastern side from its morphology. The central SMBH mass for 3C 219 is estimated by Marchesini et al. (2004) as  $6.3 \times 10^8 M_\odot$ .  $r_h$  and  $A_h$  of the western lobe are measured as 210 kpc and 5000 kpc<sup>2</sup>. From these values, the kinetic power and age are obtained as  $L_j = (0.26 - 4.3) \times 10^{47}$  ergs s<sup>-1</sup> and  $t_{\text{age}} = 37 - 150$  Myr, respectively.

Large asymmetry between the pair of lobes is observed especially in 3C 223 and 3C 284, and 3C 219. Since it seems natural to suppose that the jet properties are intrinsically symmetric and the power and age are identical on both sides, we expect that the asymmetry in the pair of lobes is due to the asymmetry and/or inhomogeneity in the ICM density profiles. Although this is an interesting subject, a further pursuit is beyond the scope of the present study. Here we assume that the actual values of  $L_j$  and  $t_{\text{age}}$  are lying in the ranges obtained from both lobes.

In Table 3 (column 4), the total kinetic powers of jet normalized by the corresponding Eddington luminosity,  $2L_j/L_{\text{Edd}}$ , are displayed. It can be seen that  $2L_j/L_{\text{Edd}}$  takes quite high values ranging from  $\sim 0.02$  to  $\sim 10$ . In exploring the physical relations between the accretion power and the outflow, the total kinetic power of jet normalized by the Eddington luminosity,  $2L_j/L_{\text{Edd}}$ , is one of the most fundamental parameters. We will return to this issue in §5.1.

## 4.2. Total internal energy vs. minimum energy

It is intriguing to compare the internal energy,  $E_c$ , deposited in the cocoon with the widely discussed energy,  $E_{\text{min}}$ , obtained from the minimum energy condition (e.g., Miley

1980).  $E_c$  is linearly proportional to the total energy injected in the cocoon ( $2L_j t_{\text{age}}$ ) and is approximately given as  $E_c \simeq L_j t_{\text{age}}$ . The dependence on the aspect ratio is given by  $E_c \propto L_j t_{\text{age}} \propto L_j^{1/2} \propto \mathcal{R}^{\alpha-4}$  (§4.1). Hence, a smaller aspect ratio (or, equivalently, a larger power) corresponds to a larger internal energy.  $E_{\text{min}}$  is the minimum value of the total energy (the sum of the energies in radiating non-thermal electrons and magnetic fields) required for a given synchrotron luminosity and is evaluated as

$$E_{\text{min}} = \frac{7}{24\pi} V_R^{3/7} \left[ 12\pi^{1/2} f(\alpha_R) (\nu_{\text{min}}^{0.5-\alpha_R} - \nu_{\text{max}}^{0.5-\alpha_R}) \nu^{\alpha_R} L_\nu \right]^{4/7} \text{ ergs}, \quad (9)$$

where  $V_R$  is the volume of the emitting region,  $\alpha_R$  is the spectral index of the synchrotron emission, and  $L_\nu$  is the synchrotron luminosity measured at frequency  $\nu$ , and  $\nu_{\text{min}}$  and  $\nu_{\text{max}}$  are the lower and higher cut-offs in the synchrotron emission, respectively.  $f(\alpha_R)$  is a function of spectral index  $\alpha_R$  which is given as

$$f(\alpha_R) \simeq \frac{3.16 \times 10^{12} (0.145)^{\alpha_R} (2\alpha_R + 1) \Gamma(\frac{\alpha_R}{2} + 1)}{(2\alpha_R - 1) \Gamma(\frac{\alpha_R}{2} + \frac{11}{6}) \Gamma(\frac{\alpha_R}{2} + \frac{1}{6}) \Gamma(\frac{\alpha_R}{2} + \frac{3}{2})},$$

where  $\Gamma$  is the Gamma function (see, e.g., Longair 1994).

The values of the spectral index  $\alpha_R$  at the low frequency band (178–750 MHz) and the flux density,  $F_\nu$ , at 178MHz are taken from Table 1 in Hardcastle et al. (1998). From the employed values of  $F_\nu$ , the synchrotron luminosities are calculated as  $L_\nu = 4\pi d_L^2 F_\nu$ , where  $d_L$  is the luminosity distance. Although  $L_\nu$  is the sum of the luminosity from lobes, jets and hot spots, no significant overestimate of  $L_\nu$  is expected because the radio emission is dominated by the lobe-component for most of FR II sources (Bridle et al. 1994; Hardcastle et al. 1998). The employed values of  $\alpha_R$ ,  $L_\nu$  and other relevant quantities are summarized in Table 2. Here we neglect the second term in Eq. (9) in deriving  $E_{\text{min}}$ , since  $\alpha_R > 0.5$  is satisfied in all sources. The lower cut-off frequency  $\nu_{\text{min}}$  is taken as  $10^4$  Hz. We will comment on this value in the next paragraph. As noted in §3.3, although GHz radio images do not show a cocoon-shape clearly and only a pair of lobes can be seen, it is known that radio images at lower frequencies reflect the cocoon shape more closely (e.g., Readhead et al. 1996; Carilli et al. 1991) because of the absence of efficient radiative coolings. Since we utilize a relatively low frequency (178MHz) band, the volume of the emission region can be approximated as  $V_R \sim V_c$ . Here we employ the median value of  $\mathcal{R}$ , i.e.  $\mathcal{R} = 0.75$ , in evaluating  $V_R$ . We define the ratio of  $E_c$  to  $E_{\text{min}}$  as  $\eta_c$ :

$$\eta_c \equiv \frac{E_c}{E_{\text{min}}}. \quad (10)$$

The obtained values of  $E_{\text{min}}$ ,  $E_c$ , and  $\eta_c$  are summarized in Table 3. We find that  $E_c$  is larger than  $E_{\text{min}}$  and  $\eta_c$  is in the range of  $4 < \eta_c < 310$ . This implies that there is a substantial

deviation from the minimum energy condition. We will discuss this topic more in detail in §5.2.

Lastly, we comment on the reliability of  $\eta_c$ . The lower cut-off frequency,  $\nu_{\min}$ , is one of the ingredients, which introduce uncertainties in  $\eta_c$  because it is difficult to determine by radio observations. The value employed above is obtained from the following relation  $\nu_{\min} \approx 10^4 (B/10^{-5} \text{ G})(\gamma_{e,\min}/10)^2 \text{ Hz}$ , where  $\gamma_{e,\min}$  is the minimum Lorentz factor of non-thermal electrons. Note that the resultant  $E_{\min}$  does not change significantly by the uncertainty in  $\nu_{\min}$  because of its weak dependence. For example, when a typical value of  $\alpha_R = 0.8$  is employed  $E_{\min} \propto (\nu_{\min}/10^4 \text{ Hz})^{6/35}$ . It should be also mentioned that the difference between the actual emission volume and the employed one, which we do not expect to vary by orders, does not affect our result, since the dependence of  $E_{\min}$  on the emission volume  $V_R$  is weak,  $E_{\min} \propto V_R^{3/7}$ . Hence the precise determination of the latter is not necessary.

### 4.3. On the estimation of $L_j$ and $E_c$

#### 4.3.1. Upper limits and lower limits

It is important to consider the validity of the over-pressure condition (i.e.  $P_c > P_a$ ), since the lower limits of  $L_j$  and  $E_c$  are determined by this condition in most cases (see Figs. 4-7). In our model, a larger  $P_c$  corresponds to a smaller  $\mathcal{R}$ . Though we explore a wide range of  $\mathcal{R}$  ( $0.5 \sim 1$ ), it is intuitively more likely that  $\mathcal{R}$  is smaller than unity, that is, the cocoon is prolate rather than spherical. Hence, the results of our analysis suggest that the sources examined in the present study are likely to be over-pressured indeed. Incidentally, the prolate shape of cocoon is endorsed by the fact that independent age estimations of Cygnus A (Carilli et al. 1991) and 3C 284 (Alexander & Leahy 1987) based on the spectral ageing method are more consistent with the results for the aspect ratio of 0.5 than for 1.0. (Unfortunately, the age estimations are not available for 3C 223 and 3C 219 in the literature).

In all cases, the maximum values of  $L_j$  and  $E_c$  correspond to the minimum value of  $\mathcal{R}$  ( $L_j \propto \mathcal{R}^{2\alpha-8}$ ). Though  $\mathcal{R} = 0.5$  is chosen as the lower limit in the present study (§3.3), the possibility of even smaller aspect ratios cannot be ruled out, since the radius of cocoon body  $r_c$  cannot be constrained very well from the radio images. It is emphasized again that smaller values of  $\mathcal{R}$  predict larger  $L_j$  and  $E_c$ .

#### 4.3.2. Kinetic energy in the cocoon

We have so far neglected the kinetic energy of bulk flows in the cocoon, assuming that the internal energy is dominated over the kinetic energy. This may be justified by the fact that the cocoon is filled with shocked jet matter, which are expected to flow subsonically. It is, however, important to estimate the possible changes in  $L_j$  and  $E_c$  that the inclusion of the kinetic energy in Eq. (3) (energy equation) may make, since our results are rather sensitive to the changes in the energy equation (see the discussion in §2.4). Although the lack of our knowledge on the mass deposited in the cocoon makes it difficult to estimate the kinetic energy quantitatively, the changes in  $L_j$  and  $E_c$  are not significant for the conclusion of the paper even in the case, where the kinetic energy is comparable to the internal energy, as shown shortly.

Just as in §2.4, the modification in energy equation is reflected in the value of the numerical factor  $\mathcal{C}_{\text{vh}}$  of Eq. (6). Note that  $\mathcal{C}_{\text{vh}}$  depends linearly on the ratio of the total internal energy to the total injected energy,  $\epsilon \equiv E_c/(2L_j t_{\text{age}})$ , which is  $\sim 1/2$  in the present study, since roughly a half of the injected energy is consumed for the  $PdV$  work. The inclusion of the kinetic energy modifies  $\epsilon$  as  $\epsilon \sim 1/(2+f)$ , where  $f$  is defined as the ratio of the kinetic energy to the internal energy and  $\mathcal{C}_{\text{vh}}$  is reduced from the value obtained in the present study by a factor of  $\sim 2/(2+f)$ . It is hence found that even if the kinetic energy is as large as the internal energy, namely  $f \sim 1$ ,  $L_j(\propto \mathcal{C}_{\text{vh}}^2)$  and  $E_c(\propto \mathcal{C}_{\text{vh}})$  are reduced only by factors of  $\sim 4/9$  and  $\sim 2/3$ , respectively. The inclusion of the kinetic energy, therefore, does not change the conclusion of this paper.

## 5. SUMMARY AND DISCUSSIONS

In this paper we have investigated the total kinetic power and age of powerful FR II jets. We have selected four FR II radio galaxies (Cygnus A, 3C 223, 3C 284, and 3C 219), for which the surrounding ICM densities and pressures are known in the literature. Below we summarize our main results.

(I) *Large fractions of the Eddington power in the range of  $\gtrsim 0.02 - 0.7$  are carried away as a kinetic power of jet in the FR II sources.*

(II) *The energy deposited in the cocoon,  $E_c$ , exceeds the minimum energy,  $E_{\text{min}}$ , by a factor of  $4 - 310$ .*

Although our results allow a wide range of  $L_j$  and  $E_c$ , interesting implications can still be obtained and will be discussed below. In §5.1., we address some issues concerning the



ratio of  $L_j$  to  $L_{\text{Edd}}$  by referring to the studies of X-ray binaries. In §5.2., the energetics in the cocoon is constrained from the obtained  $\eta_c$ .

### 5.1. $L_j/L_{\text{Edd}}$

Postulating that the relativistic jet is powered by the release of gravitational energy ( $L_{\text{acc}}$ ) of accreting matter (e.g., Marscher et al. 2002), the jet power can be expressed as  $2L_j = \epsilon_j L_{\text{acc}}$ , where  $\epsilon_j$  is the efficiency of energy conversion ( $0 < \epsilon_j < 1$ ). Hence,  $2L_j/L_{\text{Edd}}$  gives the minimum mass accretion rate normalized by the Eddington mass accretion rate. Our results then suggest that quite high mass accretion rates, at least above  $0.02L_{\text{Edd}}$ , are required to produce FR II radio sources. Moreover, since  $10 \gtrsim 2L_j/L_{\text{Edd}} \gtrsim 0.65$  is predicted for 3C 219, some FR II radio sources may have super-Eddington mass accretion rates. The theory of accretion disk predicts that the accretion disk of these objects is optically-thick and called the *slim-disk* (e.g., Abramowicz et al. 1988). From three distinctive X-ray properties (the large photon index  $\Gamma \gtrsim 2$ , rapid variability and soft X-ray excess), narrow line Seyfert 1 galaxies (NLS1s) are considered to be super-Eddington objects and, therefore, are inferred to have a slim-disk (e.g., Pounds et al. 1995; Boller et al. 1996; Mineshige et al. 2000; Collin & Kawaguchi 2004; Shemmer et al. 2006). If 3C 219 is indeed super-Eddington, it is expected to show the above mentioned X-ray features like NLS1s. Note, however, that 3C 219 has a relatively hard X-ray spectrum with  $\Gamma = 1.58 < 2$  (Shi et al. 2005), and thus the physical state of the accretion disk in 3C 219 could be different from those in NLS1s.

In order to explore the nature of the accretion disk in 3C 219, we compare the characteristics of AGNs with those of X-ray binaries (XRB), since both of them have common physical processes such as disk accretions, relativistic jets, and quenching of these jets (e.g., Heinz & Sunyaev 2003; Ho 2005; McHardy et al. 2006). Thanks to their much shorter dynamical timescales, XRBs in various states have been observed in great detail and are found to occupy particular X-ray spectral states (Fender et al. 2004; Remillard & McClintock 2006 for a review) as follows;

- (i)  $L_{\text{acc}}/L_{\text{Edd}} \lesssim 0.01$  (low/hard state: LS),
- (ii)  $0.01 \lesssim L_{\text{acc}}/L_{\text{Edd}} \lesssim 0.3$  (high/soft state: HS),
- (iii)  $L_{\text{acc}}/L_{\text{Edd}} \gtrsim 0.3$  (very high state: VHS).

State (i) is usually accompanied by a jet. For  $L_{\text{acc}}/L_{\text{Edd}} > 0.01$ , the radio emission is quenched in state (ii), while in state (iii), the soft VHS, which has an X-ray spectrum dominated by a steep power-law component (photon index  $\Gamma > 2$ ), is radio quiet and the

hard VHS and/or the transition from the hard VHS to the soft VHS is accompanied by relativistic ejection events.

If the analogy between XRBs and AGNs holds, NLS1s may be in the soft VHS, since many NLS1s have a steep power-law component and high Eddington ratios  $> 0.3$  (e.g., Collin & Kawaguchi 2004), that is, higher than the upper limit set by the stability of the Shakura & Sunyaev (1973) disk (Shakura & Sunyaev 1973). On the other hand, 3C 219 (FR II) may correspond to the hard VHS and/or the transition state because it has hard X-ray spectra and high Eddington luminosities. In order to judge whether AGNs are scaled-up XRBs, it is essential to confirm that radio loud AGNs actually have the states analogous to the spectral states (especially VHS) in XRBs<sup>1</sup>.

The co-evolution of a central black hole (BH) and its host galaxy together with AGN feedbacks have been intensively studied in various ways (e.g., Silk & Rees 1998; Di Matteo et al. 2003; Granato et al. 2004). The intensive surveys of QSOs show that the number density of QSOs is peaked at  $z \approx 2$  (Fan et al. 2001). The existence of QSOs at  $z \gtrsim 2$  with a central BH of a mass smaller than predicted from the bulge BH-mass relation is naturally expected in the build-up of SMBHs toward  $z \approx 2$ . For the exploration of the co-evolution processes, dusty spheroidal galaxies (e.g., galaxies emitting sub-millimeter radiations and ultra-luminous infrared galaxies) are the ones to be scrutinized, since the dusty-gas in them is one of the key quantities for the co-evolution. Kawakatu et al. (2003) pointed out the possibility of radio loud AGNs at high- $z$  being QSOs in the early evolution phase (we call them proto-QSOs) that contain a growing BH. It is, however, difficult to explore the nature of proto-QSOs at high- $z$  by observations in optical and X-ray bands owing to severe dust-absorptions. In contrast, the estimate of  $L_j$  and  $t_{\text{age}}$  presented in this work is applicable even to high- $z$  sources (e.g., Schmidt et al. 2006) without being suffered from the dust extinction. Therefore, the estimate of  $L_j/L_{\text{Edd}}$  based on the cocoon dynamics is a potential new powerful tool to discover proto-QSOs among high- $z$  radio loud AGNs.

## 5.2. The energetics

Lastly, we discuss the energetics in the cocoon. Summing up in advance, the total internal energy of invisible components such as thermal leptons and/or protons tends to be larger than those of radiating non-thermal electrons and magnetic fields.  $E_c$  is expressed by components as  $E_c = (U_e + U_B + U_{\text{inv}})V_c$ , where  $U_e$ ,  $U_B$ , and  $U_{\text{inv}}$  are the energy densities

---

<sup>1</sup>It has been well established that low-luminosity AGNs are the high-mass counterpart of XRBs in LS's (Ho 2005).

of non-thermal leptons (electrons and positrons), magnetic fields, and invisible particles, respectively. The energy ratio  $\eta_c \equiv E_c/E_{\min}$  can be then expressed as  $\eta_c = (U_e + U_B + U_{\text{inv}})/U_{\min}$ , where  $U_{\min} = E_{\min}/V_c$  is the minimum energy density. From the obtained values of  $\eta_c$ , we investigate here the contribution of  $U_{\text{inv}}$  to the total energy by evaluating  $U_e/U_{\min}$  and  $U_B/U_{\min}$ .

It is useful to express  $U_e/U_{\min}$  and  $U_B/U_{\min}$  in terms of  $U_e/U_B$ , since  $U_e/U_B$  has been intensively investigated by a lot of authors (e.g., Isobe et al. 2002; Kataoka et al. 2003; Croston et al. 2004; Kataoka & Stawarz 2005; Croston et al. 2005). Since the synchrotron luminosity  $L_\nu$  is proportional to  $U_e U_B^{3/4} V_c$ , we obtain the relation  $U_e \propto (U_e/U_B)^{3/7}$ , or equivalently  $U_B \propto (U_e/U_B)^{-4/7}$  for fixed values of  $L_\nu$  and  $V_c$ . From this relation and Eq. (9), we can derive the following expressions:

$$\frac{U_e}{U_{\min}} \simeq 0.5 \left( \frac{U_e}{U_B} \right)^{3/7}, \quad \frac{U_B}{U_{\min}} \simeq 0.5 \left( \frac{U_e}{U_B} \right)^{-4/7}. \quad (11)$$

Hence,  $U_{\text{inv}}/U_{\min}$  is given by

$$\frac{U_{\text{inv}}}{U_{\min}} \simeq \eta_c - 0.5 \left\{ \left( \frac{U_e}{U_B} \right)^{3/7} + \left( \frac{U_e}{U_B} \right)^{-4/7} \right\}. \quad (12)$$

Recent observations show that the ratio of  $U_e$  to  $U_B$  is  $1 \lesssim U_e/U_B \lesssim 10$  on average. Substituting these values in Eq. (11), we find  $0.13 \lesssim U_B/U_{\min} \lesssim 0.5$  and  $0.5 \lesssim U_e/U_{\min} \lesssim 1.3$ . Since the obtained range of  $\eta_c$  is  $\sim 4 - 310$ ,  $U_{\text{inv}}/U_{\min}$  is evaluated as  $3 \lesssim U_{\text{inv}}/U_{\min} \lesssim 310$  from Eq. (12). Thus, we conclude that the internal energy of invisible particles must be larger than those of radiating non-thermal leptons and magnetic fields ( $U_e, U_B \lesssim U_{\text{inv}}$ ) to explain the result obtained in this paper that  $E_c$  is larger than  $E_{\min}$  by a factor of 4 at least.

We are grateful to A. Celotti for useful comments. We thank M. Machida for useful comments and discussions on §5.1. This work was partially supported by the Grants-in-Aid for the Scientific Research (14740166, 14079202) from Ministry of Education, Science and Culture of Japan and by Grants-in-Aid for the 21th century COE program “Holistic Research and Education Center for Physics of Self-organizing Systems”. This research has made use of SAOimage DS9, developed by Smithsonian Astrophysical Observatory.

## REFERENCES

Abramowicz, M. A., Czerny, B., Laosta, J. P., & Szuszkiewicz, E. 1988, ApJ, 332, 646

- Allen, S. W., Dunn, R. J. H., Fabian, A. C., Taylor, G. B., & Reynolds, C. S. 2006, MNRAS, 372, 21
- Alexander, P., & Leahy, J. P. 1987, MNRAS, 225, 1
- Aloy, M. A., Gomez, J. L., Ibanez, J. M., Marti, J. M., & Muller, E. 2000, ApJ, 528, 85
- Begelman, M. C. 1996, Cygnus A – Study of a Radio Galaxy, 209
- Begelman, M. C., Blandford, R. D., & Rees, M. J. 1984, Rev. Mod. Phys., 56, 255
- Begelman, M. C., & Cioffi, D. F. 1989, ApJ, 345, 21
- Bicknell, G. V., Dopita, M. A., & O’Dea, C. P. 1997, ApJ, 485, 112
- Böhringer, H., Voges, W., Fabian, A. C., Edge, A. C., & Neumann, D. M. 1993, MNRAS, 264, 25
- Boller, T., Brandt, W. N., & Fink, H. 1996, A&A, 305, 53
- Bridle, A. H., Hough, D. H., Lonsdale, C. J., Burns, J. O., & Laing, R. A. 1994, AJ, 108, 766
- Carilli, C. L., & Barthel, P. D. 1996, A&A Rev, 7, 1
- Carilli, C. L., Perley, R. A., Dreher, J. W., & Leahy, J. P. 1991, ApJ, 383, 554
- Cavaliere, A., & Fusco-Femiano, R. 1978, A&A, 70, 677
- Celotti, A., & Fabian, A. C. 1993, MNRAS, 264, 228
- Cioffi, D. F., & Blondin, J. M. 1992, ApJ, 392, 458
- Clarke, D. A., Bridle, A. H., Burns, J. O., Perley, R. A., & Norman, M. L. 1992, ApJ, 385, 173
- Collin, S., & Kawaguchi, T. 2004, A&A, 426, 797
- Cox, C. I., Gull, S. F., & Scheuer, P. A. G. 1991, MNRAS, 252, 558
- Croston, J. H., Birkinshaw, M., Hardcastle, M. J., & Worrall, D. M. 2004, MNRAS, 353, 879
- Croston, J. L., Hardcastle, M. H., Harris, D. E., Besole, E., Birkinshaw, M., & Worrall, D. M. 2005, ApJ, 626, 733

- Di Matteo, T., Croft, R. A. C., Springel, V., & Hernquist, L. 2003, *ApJ*, 593, 56
- Di Matteo, T., Springel, V., & Hernquist, L. 2005, *Nature*, 433, 604
- Dunn, R. J. H., & Fabian, A. C. 2004, *MNRAS*, 355, 862
- Fabian, A. C. 1999, *MNRAS*, 308, L39
- Fabian, A. C., Celotti, A., Blundell, K. M., Kassim, N. E., & Perley, R. A. 2002, *MNRAS*, 331, 369
- Fan, X., et al. 2001, *AJ*, 122, 2833
- Fender, R. P., Belloni, T. M., & Gallo, E. 2004, *MNRAS*, 355, 1105
- Ferrarese, L., & Merritt, D. 2000, *ApJ*, 539, L9
- Gomez, J. L., Marti, J. M., Marscher, A. P., Ibanez, J. M., & Alberdi, A. 1997, *ApJ*, 482, 33
- Granato, G. L., De Zotti, G., Silva, L., Bressan, A., & Danese, L. 2004, *ApJ*, 600, 580
- Hardcastle, M. J., Alexander, P., Pooley, G. G., & Riley, M. J. 1998, *MNRAS*, 296, 445
- Hardcastle, M. J., & Worrall, D. M. 1999, *MNRAS*, 309, 969
- Hardcastle, M. J., & Worrall, D. M. 2000, *MNRAS*, 319, 562
- Ho, L. C. 2005, *Ap&SS*, 300, 219
- Isobe, N., Tashiro, M., Makishima, K., Iyomoto, N., Suzuki, M., Murakami, M. M., Mori, M., & Abe, K. 2002, *ApJ*, 580, L111
- Kaiser, C. R., & Alexander, P. 1997, *MNRAS*, 286, 215
- Kataoka, J., et al. 2003, *A&A*, 410, 833
- Kataoka, J., & Stawarz, L. 2005, *ApJ*, 622, 797
- Kauffmann, G., et al. 2003, *MNRAS*, 346, 1055
- Kawakatu, N., Umemura, M., & Mori, M. 2003, *ApJ*, 583, 85
- Kawakatu, N., & Kino, M. 2006, *MNRAS*, 370, 1513
- King, A. 2003, *ApJ*, 596, L27

- Kino, M., & Kawakatu, N. 2005, MNRAS, 364, 659
- Kino, M., Kawakatu, N., & Ito, H. 2007, MNRAS, 376, 1630
- Komissarov, S. S., & Falle, S. A. E. G. 1997, MNRAS, 288, 833
- Kormendy, J., & Richstone, D. 1995, ARA&A, 33, 581
- Kubo, H., Takahashi, T., Madejski, G., Tashiro, M., Makino, F., Inoue, S., & Takahara, F. 1998, ApJ, 504, 693
- Leahy, J. P., & Gizani, N. A. B. 2001, ApJ, 555, 709
- Leahy, J. P., & Perley, R. A. 1991, AJ, 102, 537
- Leahy, J. P., Pooley, G. G., & Riley, M. 1986, MNRAS, 222, 753
- Liu, R., Pooley, G., & Riley, J. M. 1992, MNRAS, 257, 545
- Longair, M. S. 1994, High Energy Astrophysics (Cambridge: Cambridge Univ. Press)
- Magorrian, J., et al. 1998, AJ, 115, 2285
- Marchesini, D., Celotti, A., & Ferrarese, L. 2004, MNRAS, 351, 733
- Marscher, A. P., Jorstad, S. G., Gomez, J., Aller, M. S., Terasranta, H., Lister, M. L., & Stirling, A. M. 2002, Nature, 417, 625
- McHardy, M., Koerding, E., Knigge, C., Uttley, P., & Fender, R. P. 2006, Nature, 444, 730
- Miley, G. 1980, ARA&A, 18, 16
- Miller, C. J., Nichol, R. C., Gomez, P. L., Hopkins, A. M., & Bernardi, M. 2003, ApJ, 597, 142
- Mineshige, S., Kawaguchi, T., Takeuchi, M., & Hayashida, K. 2000, PASJ, 52, 499
- Mioduszewski, A. J., Hughes, P. A., & Duncan, G. C. 1997, ApJ, 476, 649
- Perley, R. A., Dreher, J. W., & Cowan, J. J. 1984, ApJ, 285, 35
- Pounds, K. A., Done, C., & Osborne, J. P. 1995, MNRAS, 277, L5
- Rawlings, S., & Saunders, R. 1991, Nature, 349, 138

- Readhead, A. C. S., Taylor, G. B., Xu, W., Pearson, T. J., Wilkinson, P. N., & Polatidis, A. G. 1996, *ApJ*, 460, 612
- Remillard, R. A., & McClintock, J. E. 2006, *ARA&A*, 44, 49
- Reynolds, C. S., & Fabian, A. C. 1996, *MNRAS*, 278, 479
- Scheck, L., Aloy, M. A., Marti, J. M., Gomez, J. L., & Muller, E. 2002, *MNRAS*, 331, 615
- Scheuer, P. A. G. 1995, *MNRAS*, 277, 331
- Schmidt, S. J., Connolly, A. J., & Hopkins, A. M. 2006, *ApJ*, 649, 63
- Shakura, N. I., & Sunyaev, R. A. 1973, *A&A*, 24, 337
- Shemmer, O., Brandt, W. N., Netzer, H., Maiolino, R., & Kaspi, S. 2006, *ApJ*, 646, L29
- Shi, Y., et al. 2005, *ApJ*, 629, 88
- Silk, J., & Rees, M. J. 1998, *A&A*, 331, L1
- Smith, D. A., Wilson, A. S., Arnaud, K. A., Terashima, Y., & Young, A. J. 2002, *ApJ*, 565, 195
- Spiegel, D. N., et al. 2003, *ApJS*, 148, 175
- Tadhunter, C., Marconi, A., Axon, D., Wills, K., Robinson, T. G., & Jackson, N. 2003, *MNRAS*, 342, 861
- Tremaine, S., et al. 2002, *ApJ*, 574, 740
- Urry, C. M., & Padovani, P. 1995, *PASP*, 107, 803
- Willot, C. J., Rawlings, S., Blundell, K. M., & Lacy, M. 1999, *MNRAS*, 309, 1017
- Wilson, A. S., Young, A. J., & Shopbell, P. L. 2000, *ApJ*, 544, 27
- Wilson, A. S., Smith, D. A., & Young, A. J. 2006, *ApJ*, 644, L9
- Woo, J.-H., & Urry, C. M. 2002, *ApJ*, 579, 530
- Young, A. J., Wilson, A. S., Terashima, Y., Arnaud, K. A., & Smith, D. A. 2002, *ApJ*, 564, 176

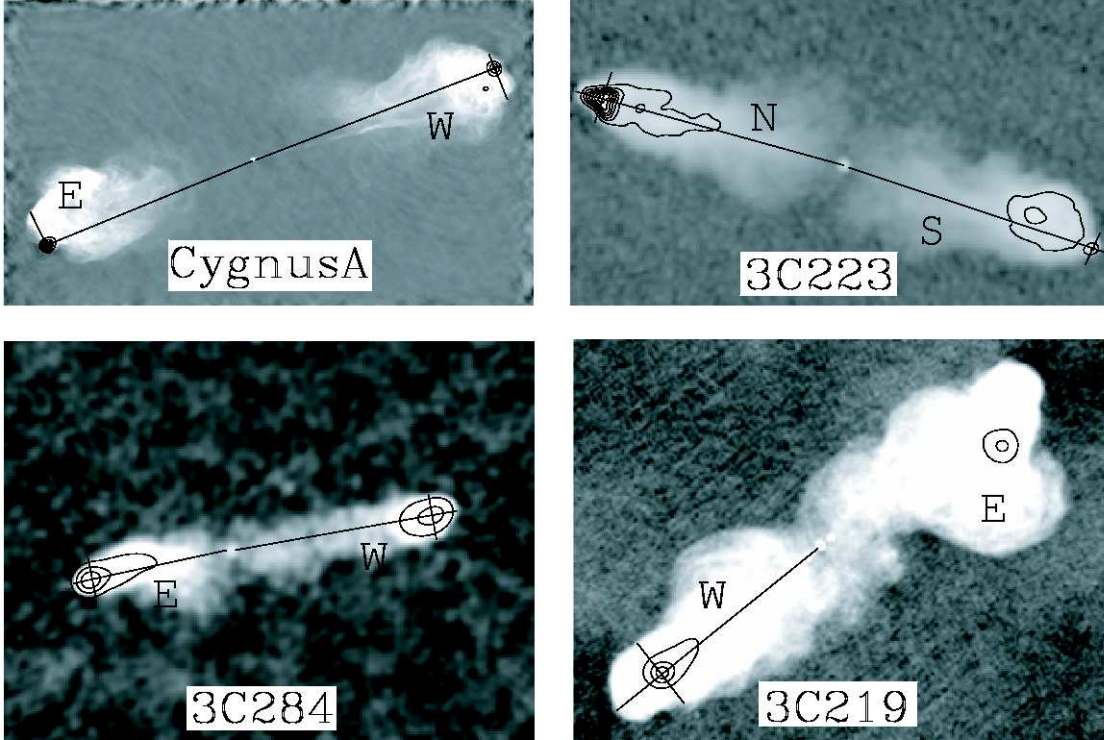


Fig. 3.— Logarithmic-scaled 5-GHz VLA map of Cygnus A (upper-left) and 1.5GHz VLA maps of 3C 223 (upper-right), 3C 284 (lower-left), and 3C 219 (lower-right) with linearly spaced contours are displayed. The straight lines overlaid in each map denote the lines we have used to measure  $r_h$  and  $A_h$ .



Table 1: The quantities measured from observations.

Source	$r_h$ (kpc)	$A_h$ (kpc <sup>2</sup> )	$\rho_a$ (g cm <sup>-3</sup> )	$P_a$ (dyne cm <sup>-2</sup> )	$\alpha$	Ref.
(1)	(2)	(3)	(4)	(5)	(6)	(7)
Cygnus A E	60	150	$8.3 \times 10^{-27}$	$8.0 \times 10^{-11}$	1.5	1,2
Cygnus A W	70	150	$6.6 \times 10^{-27}$	$6.4 \times 10^{-11}$	1.5	1,2
3C 223 N	340	4300	$5.5 \times 10^{-28}$	$1.2 \times 10^{-12}$	1.6	3
3C 223 S	340	1800	$5.5 \times 10^{-28}$	$1.2 \times 10^{-12}$	1.6	3
3C 284 E	260	4600	$4.0 \times 10^{-28}$	$6.4 \times 10^{-13}$	1.0	3
3C 284 W	380	6200	$2.3 \times 10^{-28}$	$3.7 \times 10^{-13}$	1.4	3
3C 219 W	210	5000	$1.0 \times 10^{-27}$	$1.6 \times 10^{-12}$	2.0	4

---

Note. — Column (1) shows the names of radio sources, and the following alphabet distinguishes the pair of jets (see Fig. 3). Columns (2) and (3) display, respectively, the cocoon lengths and the cross sectional areas of cocoon head measured from Fig. 3. Columns (4) and (5) give the estimated ICM densities and pressures at  $r = r_h$ . In Column(6), the estimated power-law indexes of the ICM density are presented. References for the density profiles and pressures are listed in column (7)

References. — (1) Reynolds & Fabian (1996); (2) Smith et al. (2002); (3) Croston et al. (2004);(4)Hardcastle & Worrall (1999).

Table 2: The observed radio information.

Source	z	$d_L$ (Mpc)	$F_\nu$ (Jy)	$\alpha_R$	$L_\nu$ (ergs s <sup>-1</sup> Hz <sup>-1</sup> )
(1)	(2)	(3)	(4)	(5)	(6)
Cygnus A	0.0565	249	9660	0.74	$6.2 \times 10^{35}$
3C 223	0.1368	635	16.0	0.74	$7.7 \times 10^{33}$
3C 284	0.2394	1182	12.3	0.95	$1.0 \times 10^{34}$
3C 219	0.1744	829	44.9	0.81	$3.7 \times 10^{34}$

Note. — Column (1) shows the names of radio sources. Columns (2) and (3) display, respectively, the redshift and the luminosity distance calculated for the cosmology with  $H_0 = 71 \text{ km s}^{-1}$ ,  $\Omega_M = 0.3$ , and  $\Omega_\Lambda = 0.7$ . Columns (4) and (5) give the values of flux densities and spectral indexes at 178MHz, which are taken from the table (Table 1) of Hardcastle et al. (1998). In Column (6) the calculated luminosity densities at 178MHz is presented

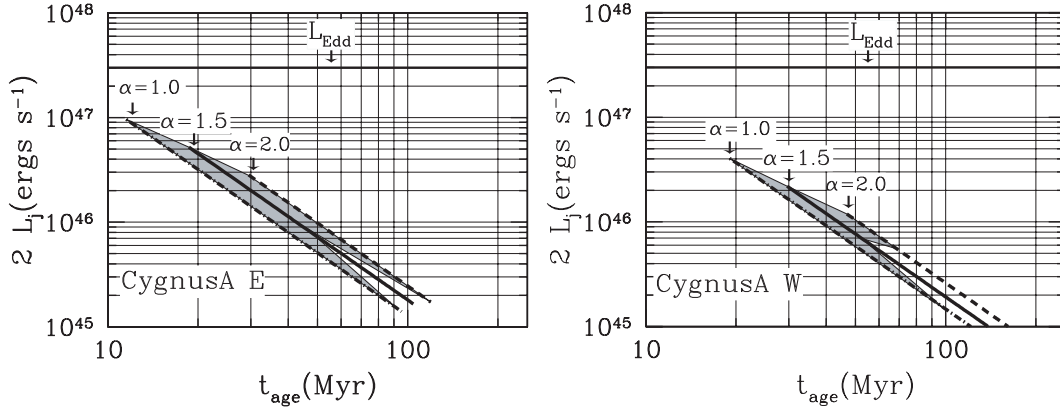


Fig. 4.— The obtained ranges of power and age of Cygnus A. The three oblique lines, which lie closely to each other are the solutions for the power-law index of the ICM density ( $\alpha$ ) shown by arrow; The solid line represents the solution for the estimated power-law index (see Table 1). The dashed and dot-dashed lines represent the solutions for the power-law index increased by 0.5 and decreased by 0.5, respectively. The shaded regions show allowed ranges where the overpressure condition ( $P_c > P_a$ ) is satisfied. Also the Eddington luminosities are displayed by the horizontal lines for comparison.

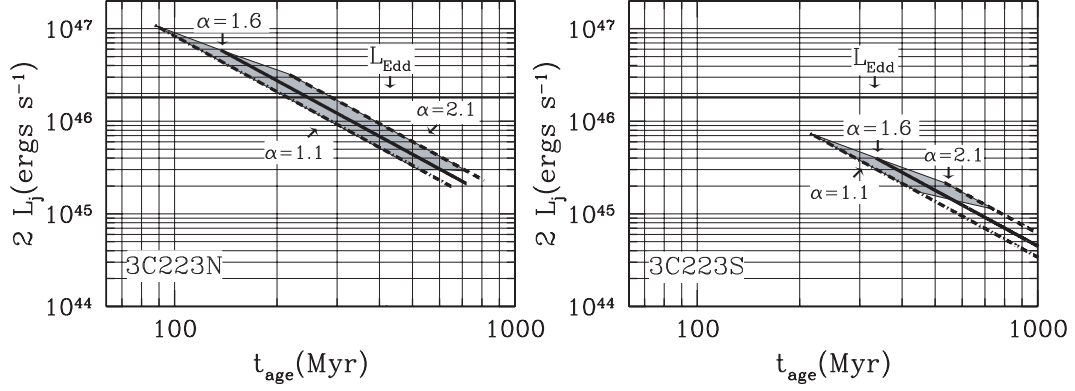


Fig. 5.— Same as Fig. 4, but for 3C 223.

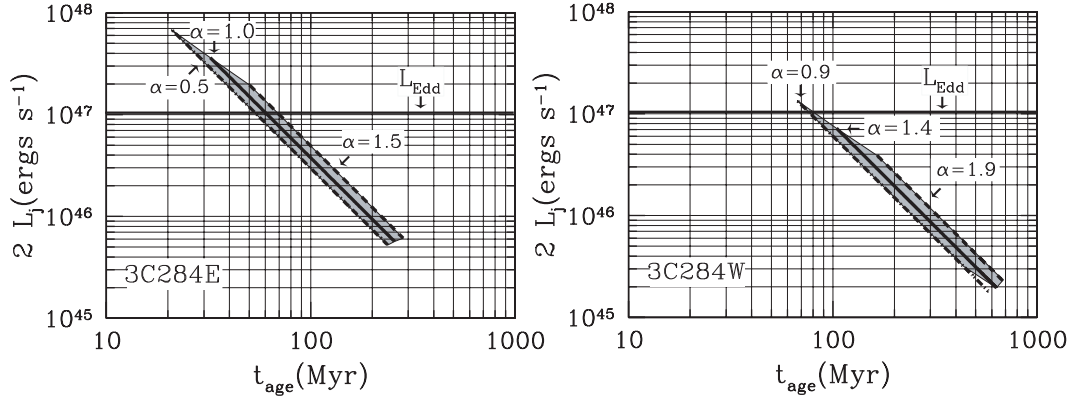


Fig. 6.— Same as Fig. 4, but for 3C 284.

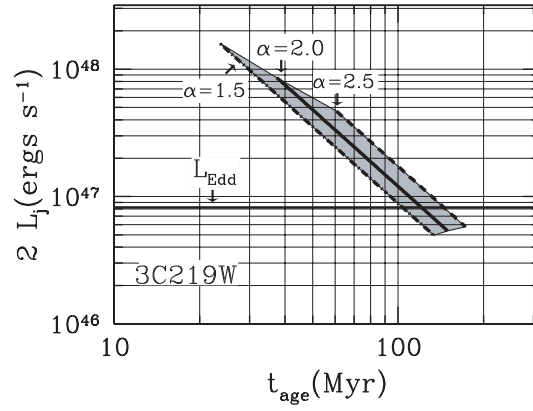


Fig. 7.— Same as Fig. 4, but for 3C 219.

Table 3. The obtained properties of the jet and the cocoon together with minimum energy of the radio lobe.

Source	$L_j$ ( $10^{46}$ ergs s $^{-1}$ )	$t_{\text{age}}$ (Myr)	$M_{\text{BH}}$ ( $M_{\odot}$ )	$2L_j/L_{\text{Edd}}$	$E_c$ ( $10^{60}$ ergs)	$E_{\text{min}}$ ( $10^{60}$ ergs)	$\eta_c$
(1)	(2)	(3)	(4)	(5)	(6)	(7)	(8)
Cygnus A E	0.4 - 2.6	19 - 47	$2.5 \times 10^9$ (2)	0.025 - 0.16	6.2 - 16	1.4	4.4 - 11
Cygnus A W	0.35 - 1.1	30 - 53	$2.5 \times 10^9$ (2)	0.021 - 0.068	6.1 - 11	1.4	4.3 - 7.8
3C 223 N	0.15 - 2.9	140 - 610	$1.4 \times 10^8$ (1)	0.16 - 3.2	30 - 130	0.88	34 - 150
3C 223 S	0.071 - 0.2	330 - 560	$1.4 \times 10^8$ (1)	0.078 - 0.22	12 - 22	0.88	14 - 25
3C 284 E	0.3 - 18	32 - 260	$8.2 \times 10^8$ (3,4)	0.053 - 3.4	26 - 210	1.8	14 - 120
3C 284 W	0.1 - 3.6	100 - 630	$8.2 \times 10^8$ (3,4)	0.018 - 0.67	21 - 130	3.0	7 - 43
3C 219 W	2.6 - 43	37 - 150	$6.3 \times 10^8$ (3)	0.65 - 10	130 - 500	1.6	79 - 310

Note. — Column (1) shows the names of radio sources, and the following alphabet distinguishes the pair of jets (see Fig. 3). Columns (2) and (3) display, respectively, the total kinetic powers and ages of the radio jets. In column (4) and (5), the black hole mass and the kinetic powers normalized by the corresponding Eddington luminosity are displayed, respectively. References for the central SMBH mass are given in parentheses. In Columns (6) and (7), the total energies deposited in the cocoon and the minimum energies required for the synchrotron emission are displayed, respectively. Column (8) gives the ratios between  $E_c$  and  $E_{\text{min}}$ .

References. — (1) Woo & Urry (2002); (2) Tadhunter et al. (2003); (3) Marchesini et al. (2004); (4) Shi et al. (2005).